ISSN 1027-4510, Journal of Surface Investigation: X-ray, Synchrotron and Neutron Techniques, 2019, Vol. 13, No. 5, pp. 787–792. © Pleiades Publishing, Ltd., 2019.
Russian Text © The Author(s), 2019, published in Poverkhnost', 2019, No. 9, pp. 3–9.

Zirconium-Based Metal-Organic UiO-66, UiO-66-NDC and MOF-801 Frameworks. Influence of the Linker Effect on the Hydrogen Sorption Efficiency

K. S. Vetlitsyna-Novikova[a, *], V. V. Butova[a, **], I. A. Pankin[a, b], V. V. Shapovalov[a], and A. V. Soldatov[a]

[a] *International Research Institute of Smart Materials, Southern Federal University, Rostov-on-Don, 344090 Russia*
[b] *Department of Chemistry and NIS Interdepartmental Center, University of Torino, I-10125 Torino, Italy*
**e-mail: kristinavetlitsyna@gmail.com*
***e-mail: butovav86@gmail.com*

Received December 29, 2018; revised February 5, 2019; accepted February 16, 2019

Abstract—Metal-organic UiO-66, UiO-66-NDC, and MOF-801 frameworks (MOFs) are produced via the solvothermal synthesis technique. The frameworks are composed of $Zr_6O_4(OH)_4$ clusters that are connected with appropriate linkers, as follows: UiO-66—terephthalic acid; UiO-66-NDC—1,4-naphthalenedicarboxilic acid; and MOF-801—fumaric acid. The single-phase composition of the samples is confirmed by X-ray powder diffraction. The identification of $Zr_6O_4(OH)_4$ clusters in all the synthesized MOFs is established using X-ray adsorption spectroscopy. The specific surface areas of UiO-66, UiO-66-NDC, and MOF-801 are evaluated, and their hydrogen adsorption–desorption isotherms are measured at 77 K, as well. Comprehensive preliminary characterization of the samples, together with hydrogen-storage-capacity data, allows one to make the following conclusions: (i) at relatively high pressures, the highest hydrogen-storage capacity is found for UiO-66 with the largest specific surface area; (ii) at relatively low pressures, MOF-801 with the smallest pores possesses the optimal structure for hydrogen sorption; (iii) a large π-system of aromatic UiO-66-NDC rings yields effective hydrogen sorption at low pressures, which is retained in pores during desorption.

Keywords: UiO-66, MOF-801, UiO-66-NDC, metal-organic framework, hydrogen storage, adsorbent, porous material

DOI: 10.1134/S1027451019050173

INTRODUCTION

Metal-organic frameworks (MOFs) belong to a class of porous materials with a high specific surface area [1–3]. MOFs are composed of secondary structural units, linked by organic molecules (linkers) in a three-dimensional frame. Secondary structural units may possess different coordinations, being presented by an individual metal ion or a complex ion cluster, as well as by a one-, two- or three-dimensional inorganic substructure [4]. This module structure allows the MOF frame to vary in wide ranges. There is one method for modifying the structure and properties of MOFs, which consists in obtaining new structures, composed of the same secondary structural units and different linkers. Linkers can be chosen so that MOFs have identical symmetry, but diverse pore sizes and functional groups. For example, this technique enabled UiO-66/UiO-67/UiO-68 MOFs to be obtained in 2008 [5, 6]. The crystal lattice of UiO contains $Zr_6O_4(OH)_4$ clusters in its sites. These can merge into a 3D frame using various linkers. It is worth mentioning that a peculiar feature of this family of materials is exclusive thermal and chemical stability. Together with a high porosity, this makes MOFs very attractive in a wide range of applications [7–10], such as gas storage.

In this respect, the possibility of hydrogen storage in UiO-66, UiO-67, UiO-66$(OH)_2$, and UIO-66(H_2ADC) MOFs was studied [7, 11–13]. Although the most obvious way of improving the hydrogen-storage capacity via increasing the specific surface area has been repeatedly tested, it has however been shown to be efficient at only high pressures and low temperatures [7]. This circumstance inhibits practical application of this kind of materials. Recent methods of increasing the hydrogen-storage capacity in MOFs are based on using suitable substituents and the optimal pore size [12–14]. Among the best candidates for hydrogen storage is zirconium fumarate MOF-801. Promising MOFs for hydrogen storage, such as UiO-66, UiO-67 and MOF-801, have been studied using theoretical approaches [14]. MOF-801 was shown to be the most efficient sorbent at low pressures.

An analog of UiO-66—9,10-anthracen dicarboxylate as a linker of UIO-66(H_2ADC)—was obtained in

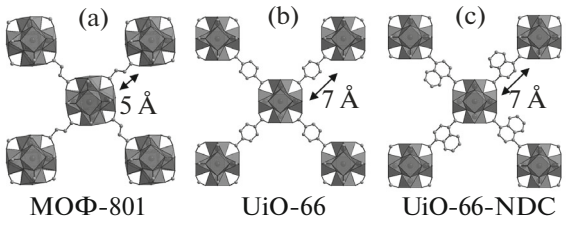

Fig. 1. Model MOF structures: (a) MOF-801, (b) UiO-66, (c) UiO-66-NDC. The arrows are completed by linker lengths that determine the MOF finite pore sizes.

work [13]. Its high hydrogen-storage capacity was interpreted in terms of an extended π system that increases substantially the enthalpy of hydrogen adsorption.

The present work is aimed at a comparative analysis of three promising MOFs: UiO-66, UiO-66-NDC and MOF-801 (Fig. 1).

The MOFs are synthesized and thoroughly characterized. By varying the linkers and pore size, an estimate of their influence on the hydrogen-storage capacity at low pressures can be obtained.

EXPERIMENTAL

Synthesis. Initial reagents, such as $ZrCl_4$, 1,4-benzenedicarboxylic acid (BDC), 1,4-naphthalenedicarboxylic acid (NDC), fumaric acid (FC), DMFA, and dichloromethane (CH_2Cl_2) (AlfaAesar Corp.), were used without subjecting them to additional purification. Deionized water was obtained from water distilled using a Simplicity UV system. During synthesis, zirconium tetrachloride ($ZrCl_4$) was solved in DMFA in a 50-mL weighing cup. The solution was then diluted with water whilst being stirred. After that, the corresponding linker (BDC, NDC and FC) was added depending on the MOF (UiO-66, UiO-66-NDC, or MOF-801). Once a transparent solution was obtained, the weighing cup was covered with a glass lid and placed in a pre-heated oven. Synthesis was conducted for a day (in the case of UiO-66 and UiO-66-NDC) and for 2 h (for MOF-801) under steady-state conditions. The synthesis temperature was 120°C. The powders were then separated by centrifugation, thoroughly rinsed with DMFA and dichloromethane, and dried in air at 60°C for 16 h. The molar ratios of the initial components were as follows: $n[ZrCl_4] : n[\text{linker}] : n[H_2O] : n[\text{DMFA}] = 1 : 1 : 3 : 300$.

Characterization techniques. The powder X-ray diffraction experiments were carried out using a Bruker D2 PHASER diffractometer. The samples were scanned by a CuK_α-radiation beam ($\lambda = 1.5417$ Å) at a step of $2\theta = 0.02°$ in the 2θ range of 5° to 50°. The specific surface area was determined using an ASAP2020 Micromeritics device. Prior to measurements, the powders were exposed to degassing by heating to 150°C under dynamic vacuum conditions for 24 h. The nitrogen and hydrogen adsorption isotherms were recorded at 196°C.

The Zr *K*-edge X-ray absorption spectra were collected using a Rigaku R-XAS Looper X-ray laboratory spectrometer. The X-ray radiation source was an X-ray tube, equipped with a tungsten cathode and anode. The working current applied to the tube was 70 mA and the working voltage was kept at 26 kV. The monochromator was a Si(840) (Johansson-type) bent crystal, ensuring an energy resolution on the order of magnitude of 2 eV at energies of 17.8–18.4 keV. The measurements were performed at room temperature in the standard Laue geometry. The detectors were an ionizing chamber filled with Ar under a pressure of 300 mbar and an SC-70 X-ray scintillating detector that enabled the beam intensity to be recorded before and after interaction with a sample, respectively. In order to achieve a high degree of homogeneity, the powdered samples were compacted into tablets with a diameter of 13 mm.

RESULTS AND DISCUSSION

X-ray powder diffraction profiles of the samples are shown in Fig. 2. All three samples are single-phase materials, whose structure corresponds to that earlier described in works [5, 10, 15]. Samples UiO-66-NDC and UiO-66 have a similar crystal structure and, consequently, X-ray diffraction profiles. Nevertheless, one can mention the higher degree of crystallinity of the UiO-66 sample in comparison with UiO-66-NDC, which is due to the structural features of the latter. Each linker of UiO-66-NDC has an additional benzene ring inside the octahedral cavity of the framework. With that, the cavity size is insufficient to arrange aromatic rings of the NDC linker in accordance with the plane of symmetry (as for UiO-66). NDC molecules are randomly displaced from the plane of symmetry by rotation about some angle around the axis of σ bonds of the aromatic ring with carboxyl groups [10]. Thus, the cubic lattice parameter *a* increases, slightly reducing the degree of crystallinity of the sample. As for MOF-801, one can see that the theoretical X-ray profile of this type of MOF is different from that of UiO-66. While the UiO-66 structure is described by a face-centered-cubic lattice of the $Fm\bar{3}m$ space group (225), the structure of MOF-801 is characterized by a primitive cubic lattice with the $Pn\bar{3}$ space group (201) (Table 1). This is due to the nonlinear arrangement of carboxyl groups in a FC molecule, resulting in the bent shape of the linker because of a double bond. Hence, secondary structural units in $Zr_6O_4(OH)_4$ MOF-801 are inclined relative to the direct position in UiO-66, where both halves are tilted opposite to each other [16].

In order to investigate possible changes in the local atomic structure of secondary structural units in the

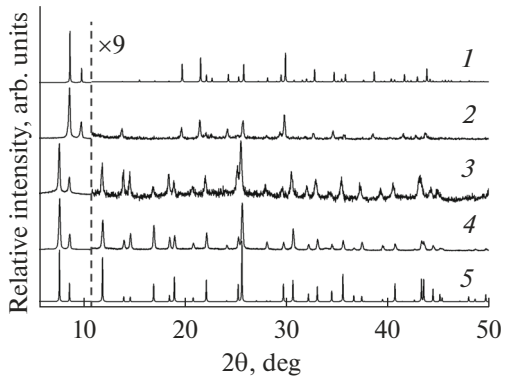

Fig. 2. X-ray diffraction profiles of (*2*) MOF-801, (*3*) UiO-66-NDC, (*4*) UiO-66. The profiles are displaced relative to the *y* axis; the peak intensities after the dotted line are multiplied by a factor of 9. The XRD profiles, given for reference—(*5*) UiO-66 P and (1) MOF-801 P—are calculated from CCDC 733458 [5] and COD 4121459 [15] crystallographic data, respectively.

synthesized MOFs, their Zr *K*-edge absorption spectra were recorded. As seen in Fig. 3, the X-ray absorption near edge structure (XANES) spectra exhibit no pronounced variations in their profiles. This is testimony to the high degree of similarity of the relative angular and radial arrangements of neighboring atoms of oxygen and zirconium in the nearest surrounding of absorbing zirconium atoms.

Furthermore, the qualitative analysis of extended X-ray absorption fine structure (EXAFS) spectra, which are only sensitive to changes in bond lengths, and not to angles, reveals that neither the additional benzene ring inside the framework pores of UiO-66-NDC, nor the displacement of secondary structural units for MOF-801 causes a noticeable variation in the bond length. Moreover, the contribution to the EXAFS-signal, corresponding to the first and second coordination spheres of Zr atoms, is due predominantly to the single scattering paths of Zr–O and Zr–Zr. Qualitative analysis of the EXAFS data is difficult because of poor-quality spectra, recorded by the laboratory X-ray spectrometer, as well as due to a large set of fitting parameters, on account of the uniqueness of the UiO-66 and MOF-801 MOF structures.

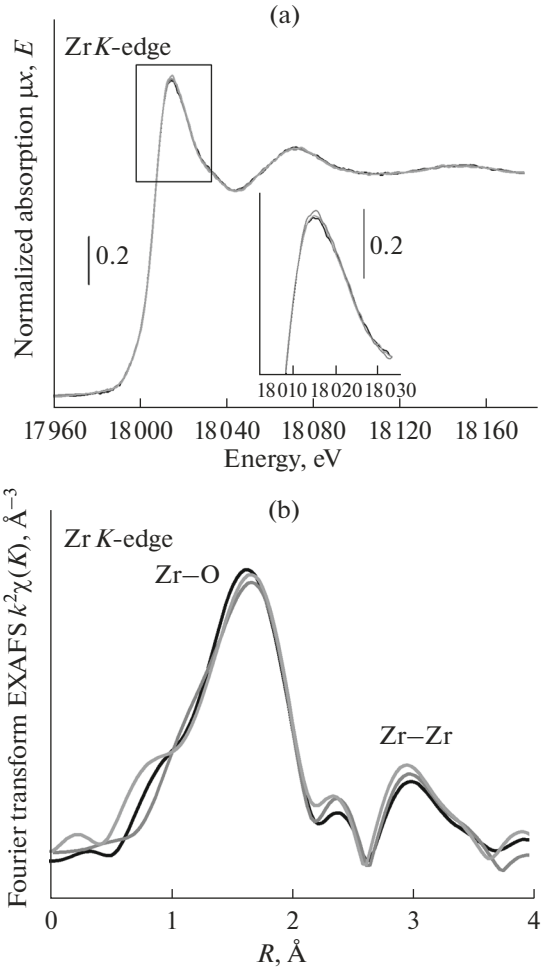

Fig. 3. a—Zr *K*-edge XANES absorption spectra; b—k_2 weighed Fourier transform (FT) modules of the EXAFS signal $\chi(k)$ without phase correction, obtained for UiO-66 (black curve), UiO-66-NDC (dark gray curve) and MOF-801 (gray curve).

The observations are consistent with data acquired earlier for UiO-66 MOF. It was shown that even a high linker-loss defect concentration leads to no visual changes in the experimental XANES spectra [10]. In this case, one can conclude that structural variations in the further atomic ordering of secondary structural

Table 1. Nitrogen adsorption, measured for various MOFs

Sample	Specific surface area, m^2/g*	Symmetry group	Unit-cell parameters**		Hydrogen-storage capacity, wt % H_2	
			a, Å	*V*, Å^3	at 20 mm Hg	at 600 mm Hg
UiO-66	941.1	$Fm\bar{3}m$ (225)	20.7330(10)	8912.2(8)	0.26	1.41
UiO-66-NDC	551.5	$Fm\bar{3}m$ (225)	20.8279(16)	9035.1(12)	0.22	0.77
MOF-801	441.6	$Pn\bar{3}$ (201)	17.9396(7)	5773.5(4)	0.28	1.22

* Specific surface area was calculated via the BET technique [23].
** Profile analysis was conducted using the Jana2006 software package.

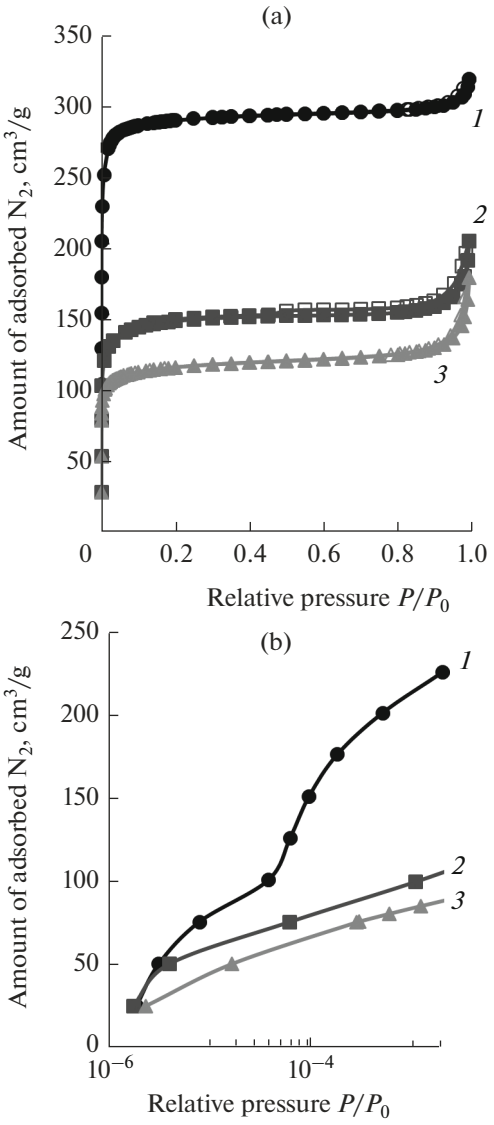

Fig. 4. (a)Nitrogen adsorption and desorption of UiO-66 (*1*), UiO-66-NDC (*2*) and MOF-801 (*3*). The adsorption branches are denoted by filled symbols and desorption branches are shown by empty ones; (b) plot of nitrogen adsorption isotherms at low pressures. The abscissa axis in (a) corresponds to a linear scale of relative pressures, whereas in (b) it corresponds to the logarithmic scale of relative pressures.

units in MOF-801 in comparison with UiO-66 and UiO-66-NDC cause no noticeable changes in the X-ray absorption spectra in both the XANES and EXAFS ranges due to the similar local atomic structure of $Zr_6O_4(OH)_4$ clusters.

The nitrogen adsorption and desorption isotherms of UiO-66, UiO-66-NDC and MOF-801 are given in Fig. 4a. All three adsorption isotherms exhibit a similar shape, characteristic of microporous materials [17]. The slight hysteresis loops in the region of relative pressures P/P_0 close to one seem to be due to nitrogen condensation in the spaces between individual crystals of the sample [10]. Approaching the low relative pressure range (Fig. 4b), one can mention the fundamentally different adsorption isotherms: while UiO-66 exhibits two well pronounced steps, the two other samples have a single bend. A similar multistep isotherm was already described for various MOFs [18–22]. For UiO-66, this phenomenon was interpreted in terms of the successive filling of octahedral and tetrahedral pores, or by an increase in the input window in the pore because of the linker's rotation upon reaching a certain pressure [21, 22]. For UiO-66-NDC, the linkers are initially rotated relative to the perfect position, which explains the lack of steps in the low-pressure adsorption isotherm. In the case of MOF-801, the linker has no aromatic rings, and a change in its position will cause no variation in the input hole sizes in the pores.

For the UiO-66, UiO-66-NDC and MOF-801 samples, the specific surface areas were calculated in accordance with the BET model (Table 1) [23]. These MOFs possess two (tetrahedral and octahedral) types of pores, whose dimensions depend on the linker length. The pore size of UiO-66 is commensurate with that in UiO-66-NDC, because the distance between the two carboxyl groups remains unchanged. The octahedral pores are ~8.4 Å in size, whereas the tetrahedral pores are 7.4 Å in size [15]. Although the pore size remains unchanged during the transition from a BDC linker to NDC, the available volume in the pore within UiO-66-NDC MOF is much lower because of the additional benzene ring, which occupies a significant amount of the pore space. This leads to a decrease in the specific surface area (Table 1). The low symmetry of MOF-801 results in two types of tetrahedral pores with close sizes (5.6 and 4.8 Å), as well as octahedral pores with diameters of 7.4 Å [15]. Both the tetrahedral and octahedral pores in MOF-801 are smaller than those in UiO-66 because of the smaller linker length, which explains the lower specific surface areas, as well as the available pore volume (Table 1).

The transition from nitrogen-type to hydrogen-type adsorption makes a big difference (Fig. 5). The low-pressure H_2 adsorption isotherm of UiO-66 does not exhibit a stepped shape, unlike the case of N_2. This phenomenon is due to the smaller radius of H_2 molecules in comparison with N_2 molecules: even in a "close" linker position the window size in the pore is enough to let hydrogen molecules penetrate without creating any steric hindrance.

If the pressure is below 5–6 mm Hg, then the most efficient hydrogen sorbent is MOF-801, followed by UiO-66-NDC and then UiO-66 (inset in Fig. 5a). The higher-pressure adsorption isotherm of UiO-66-NDC is smoother, resulting in a lower sorption capability of the material. In turn, MOF-801 at its lowest specific surface area is able to retain its advantage over UiO-66 up to 56 mm Hg. This phenomenon is due to

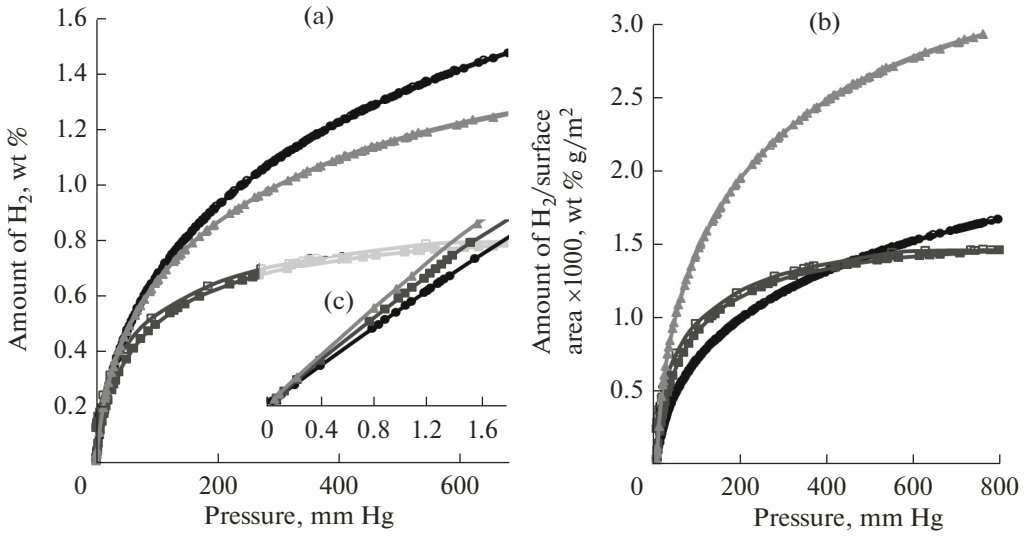

Fig. 5. (a) Nitrogen adsorption and desorption isotherms, (b) normalized isotherms of UiO-66 (black circles), UiO-66-NDC (dark gray squares) and MOF-801 (gray triangles). The adsorption branches are designated by filled symbols, and the desorption branches are given by empty ones. The inset shows the low pressure range.

the mechanism of adsorption in microporous materials. As is known, micropores can be filled at a very low relative pressure (P/P_0) because of the gas—solid state interaction. This leads to the formation of a gas-molecule single layer, covering the micropore surface. The further filling of pores allows a gas molecule to be placed between the single layers at the center of the pore, and the adsorption efficiency is hence determined by the interaction between the adsorbed gas molecules. Thus, the smaller pores are filled first, and the larger pores are filled at a higher pressure. The greater the gas-molecule size, the lower the amount of molecules needed to create a single layer. In this case, the adsorption efficiency is first of all determined by the interaction between the adsorbed gas molecules, whereas the H_2 molecule gives priority to the gas—solid state interaction and to smaller pores because of the extremely small size of its molecules. The greater efficiency of MOF-801 for hydrogen sorption becomes more evident, if we compare the effective porosity for each of the discussed materials. For this, the amount of adsorbed hydrogen is normalized to the specific surface area of the MOF. This yields a higher efficiency of MOF-801 in the whole range of considered pressures (Fig. 5b). Hence, a comparative analysis of MOF-801 and UiO-66 reveals that larger pores increase the hydrogen-storage capacity only at pressures above 55–56 mm Hg, whereas the low-pressure efficient sorbents are MOFs with small pores. We can also mention the presence of a small hysteresis loop in the adsorption curve of UiO-66-NDC, although the adsorption and desorption branches completely merge for the two other MOFs. This phenomenon is interpreted in terms of the interaction between an adsorbed hydrogen molecule and the extended π system of the naphthalene ring. The latter allows the molecule to be retained in the pore at decreasing pressure, as confirmed by theoretical simulation [24].

CONCLUSIONS

Three MOFs were synthesized and analyzed in terms of hydrogen storage. At relatively high pressures, the specific surface area and the pore size of the MOFs were shown to be of greatest importance. At pressures above 55 mm Hg, UiO-66 with the largest volume and largest pore size was found to be the most efficient sorbent for hydrogen storage. Meanwhile, from a practical point of view, the most significant characteristic is the ability to adsorb hydrogen at comparatively low pressures. To solve this problem, it is important to choose the optimum pore size, as shown by the example of MOF-801. The latter was shown to be the most efficient sorbent among the above MOFs due to the presence of a large volume of available small pores. It is also worth mentioning that an extended system of π bonds also allows adsorbed hydrogen molecules to be retained in the pores.

FUNDING

This work was supported by the Ministry of Education and Science of the Russian Federation (project no. 16.3871.2017/4.6).

REFERENCES

1. H. Furukawa, K. E. Cordova, M. O' Keeffe, et al., Science **341** (6149), 1230444 (2013). https://doi.org/10.1126/science.1230444

2. J. R. Li, R. J. Kuppler, and H. C. Zhou, Chem. Soc. Rev. **38** (5), 1477 (2009). https://doi.org/10.1039/B802426J
3. V. V. Butova, M. A. Soldatov, A. A. Guda, et al., Russ. Chem. Rev. **85** (3), 280 (2016). https://doi.org/10.1070/RCR4554
4. M. Eddaoudi, D. B. Moler, H. L. Li, et al., Acc. Chem. Res. **34** (4), 319 (2001). https://doi.org/10.1021/ar000034b
5. J. H. Cavka, S. Jakobsen, U. Olsbye, et al., J. Am. Chem. Soc. **130** (42), 13850 (2008). https://doi.org/10.1021/ja8057953
6. L. Valenzano, B. Civalleri, S. Chavan, et al., Chem. Mater. **23** (7), 1700 (2011). https://doi.org/10.1021/cm1022882
7. S. Chavan, J. G. Vitillo, D. Gianolio, et al., Phys. Chem. Chem. Phys. **14** (5), 1614 (2012). https://doi.org/10.1039/C1CP23434J
8. J. R. Li, J. Sculley, and H. C. Zhou, Chem. Rev. **112** (2), 869 (2012). https://doi.org/10.1021/cr200190s
9. S. Chavan, J. G. Vitillo, M. J. Uddin, et al., Chem. Mater. **22** (16), 4602 (2010). https://doi.org/10.1021/cm1005899
10. V. V. Butova, A. P. Budnyk, A. A. Guda, et al., Cryst. Growth Des. **17** (10), 5422 (2017). https://doi.org/10.1021/acs.cgd.7b00892
11. H. R. Abid, H. Y. Tian, H. M. Ang, et al., Chem. Eng. J. **187,** 415 (2012). https://doi.org/10.1016/j.cej.2012.01.104
12. S. S. Chen, J. Liu, Y. F. Xu, et al., Int. J. Hydrogen Energy **43** (32), 15370 (2018). https://doi.org/10.1016/j.ijhydene.2018.06.106
13. S. S. Chen, S. B. Xiao, J. Liu, et al., J. Porous Mater. **25** (6), 1783 (2018). https://doi.org/10.1007/s10934-018-0591-6
14. L. Z. Xia and F. L. Wang, Inorg. Chim. Acta **444,** 186 (2016). https://doi.org/10.1016/j.ica.2016.01.039
15. H. Furukawa, F. Gandara, Y. B. Zhang, et al., J. Am. Chem. Soc. **136** (11), 4369 (2014). https://doi.org/10.1021/ja500330a
16. G. Wissmann, A. Schaate, S. Lilienthal, et al., Microporous Mesoporous Mater **152,** 64 (2012). https://doi.org/10.1016/j.micromeso.2011.12.010
17. K. S. W. Sing, D. H. Everett, R. A. W. Haul, et al., Pure Appl. Chem. **57** (4), 603 (1985). https://doi.org/10.1351/pac198557040603
18. K. S. Park, Z. Ni, A. P. Cote, et al., Proc. Natl. Acad. Sci. USA **103** (27), 10186 (2006). https://doi.org/10.1073/pnas.0602439103
19. D. Fairen-Jimenez, S. A. Moggach, M. T. Wharmby, et al., J. Am. Chem. Soc. **133** (23), 8900 (2011). https://doi.org/10.1021/ja202154j
20. V. V. Butova, A. P. Budnyk, E. A. Bulanova, et al., Solid State Sci. **69,** 1016 (2017). https://doi.org/10.1016/j.solidstatesciences.2017.05.002
21. J. Y. Chung, C. W. Liao, Y. W. Chang, et al., J. Phys. Chem. **121** (49), 27369. https://doi.org/10.1021/acs.jpcc.7b10526
22. S. Friebe, B. Geppert, F. Steinbach, et al., ACS Appl. Mater. Interfaces **9** (14), 12878 (2017). https://doi.org/10.1021/acsami.7b02105
23. S. Brunauer, P. H. Emmett, and E. Teller, J. Am. Chem. Soc. **60,** 309 (1938). https://doi.org/10.1021/ja01269a023
24. V. V. Butova, A. P. Budnyk, K. M. Charykov, et al., Inorg. Chem. **58** (2), 1607 (2019). https://doi.org/10.1021/acs.inorgchem.8b03087

Translated by O. Maslova